Contents lists available at ScienceDirect

Organic Electronics

journal homepage: www.elsevier.com/locate/orgel

Investigation of electron transport properties in Li_2CO_3-doped $Bepp_2$ thin films

Y.P. Wang [a], X.F. Qiao [a], D.Z. Yang [a], J.Y. Huang [a], J.S. Chen [a], D.G. Ma [a,*], L.S. Dong [b,*]

[a] State Key Laboratory of Polymer Physics and Chemistry, Changchun Institute of Applied Chemistry, Chinese Academy of Sciences, University of Chinese Academy of Sciences, Changchun 130022, People's Republic of China

[b] Key Laboratory of Polymer Ecomaterials, Changchun Institute of Applied Chemistry, Chinese Academy of Sciences, University of Chinese Academy of Sciences, Changchun 130022, People's Republic of China

ARTICLE INFO

Article history:
Received 3 February 2015
Received in revised form 17 June 2015
Accepted 10 July 2015
Available online 16 July 2015

Keywords:
Electron transport
Li_2CO_3-doped $Bepp_2$ films
Admittance spectroscopy

ABSTRACT

The admittance spectroscopy investigations showed that doping lithium carbonate (Li_2CO_3) into bis[2-(2-hydroxyphenyl)-pyridine] beryllium ($Bepp_2$) greatly improved the electron mobility compared with the pure $Bepp_2$ film. The electron mobility reaches the orders of $\sim 10^{-4}$ cm^2 V^{-1} s^{-1}, almost independent of the electric field. The trap states at low frequencies were clearly observed by capacitance–frequency measurement. The current–voltage and current–thickness characteristics indicated the electron conduction of space-charge-limited current (SCLC) with discrete trap distributions in the intermediate voltage and the SCLC with exponential trap distribution at the higher voltage in the Li_2CO_3-doped $Bepp_2$ film. We further estimated the density of trap states to be about 4.54×10^{17} cm^{-3} by the temperature dependent current density characteristics. The investigation of ultraviolet photoemission spectroscopy (UPS) and X-ray photoemission spectroscopy (XPS) found that there occurs complicated chemical reaction between $Bepp_2$ and Li_2CO_3, and the $Bepp_2$ traps more electrons after Li_2CO_3 doping. This is an effective charge transfer between $Bepp_2$ and Li_2CO_3, which greatly reduces the electron injection barrier and significantly enhances the electron mobility.

1. Introduction

A considerable research efforts on organic semiconductors have recently been attached by the potential application prospect for low-cost, large area and light weight optoelectronic devices, such as organic light-emitting diodes (OLEDs) [1–4], organic solar cells (OSCs) [5,6] and organic thin film transistors (OTFTs) [7–10]. In general, there are two critical factors to improve the organic device performance: (1) enhancing the carrier injection and transport abilities; (2) keeping the charge balance. An immense effort has been made to design and synthesize organic semiconductor materials with good carrier transport abilities, especially those with high electron mobility. However, the electron mobility is typically lower than that of the hole for these materials. Therefore, it is important to improve the electron injection and transport for charge balance in organic devices.

Recently, electrical doping in organic semiconductors has been considerably accepted because it can enhance the charge injection and transport, thus improving device performance [11–14]. Alkali metal compounds, such as cesium carbonate (Cs_2CO_3) [14–16] and Li_2CO_3 [13,17] are the widely studied n-type dopants in electron transport layers. Zhao et al. [14] investigated the effect of Cs_2CO_3 doping on the electron transport properties of 4,7-diphenyl-1,10-phenanthroline (BPhen) in OLEDs, which showed that the incorporation of Cs_2CO_3 decreases the activation energy of the BPhen, resulting in the enhancement of electron injection and transport by the reduction of injection barrier and the increase of BPhen conductivity. Clearly, although the utilization of these doped films can greatly improve the performance of organic devices, the research on the charge transport properties is still not clarified. Notably, the admittance spectroscopy (AS) measurements are a feasible and powerful tool in evaluating not only the hole transport property but also the electron transport property in organic semiconductors [18–23]. In this work, we investigated in detail the electron transport properties and mechanism in Li_2CO_3-doped bis[2-(2-hydroxyphenyl)-pyridine] beryllium ($Bepp_2$) thin films by frequency-dependent admittance spectroscopy, current–voltage characteristics, ultraviolet photoemission spectroscopy (UPS) and X-ray photoemission spectroscopy (XPS).

* Corresponding authors.
E-mail addresses: mdg1014@ciac.jl.cn (D.G. Ma), dongls@ciac.jl.cn (L.S. Dong).

http://dx.doi.org/10.1016/j.orgel.2015.07.023
1566-1199/

2. Experimental

A series of electron-only devices were fabricated on glass substrates. Prior to deposition, the substrate was thoroughly cleaned in an ultrasonic bath using subsequently detergents and deionized water. The device structure was aluminum (Al)/Li_2CO_3 (1 nm)/$Bepp_2$: 3% Li_2CO_3 (100–260 nm)/Li_2CO_3 (1 nm)/Al. Here, the doping weight percentages have been optimized in the $Bepp_2$:Li_2CO_3 films. Li_2CO_3 and $Bepp_2$:Li_2CO_3 layers were grown in succession by thermal evaporation without breaking vacuum ($\sim 4 \times 10^{-4}$ Pa). The interfacial layer Li_2CO_3 was used at both sides of electrodes to guarantee the Ohmic injection of electrons, which is the basic requirement of using AS to measure the mobility of organic thin films. The Al electrodes were deposited on the substrates through shadow masks. The active area of device is 16 mm^2. The current–voltage (J–V) characteristics were carried out using a Keithley 2400 sourcemeter integrated with a vacuum cryostat (Optistat DN-V, Oxford Instruments). The AS of the fabricated devices was measured at room temperature by using an Agilent E4980A precision LCR meter in the frequency range of 50 Hz–3 MHz with the oscillation amplitude of the ac voltage kept at 100 mV. The temperature-dependent AS was measured by a vacuum cryostat (Optistat DN-V, Oxford Instruments) in the temperature range of 140–300 K. UPS was carried out using a helium discharge lamp (HeI α = 21.2 eV) and a hemispherical energy analyzer (Specs PHOIBOS 150). XPS study was performed with Al $K\alpha$ X-ray source (1486.6 eV, Thermo Electron Corporation, ESCALAB 250).

3. Results and discussion

3.1. Current–voltage characteristics and temperature dependence

The current density (J) versus voltage (V) plots of Li_2CO_3-doped $Bepp_2$ films with different thicknesses (d) at a given voltage at room temperature are shown in Fig. 1. It can be seen that the current density increases with decreasing the film thickness. For the doping film of d = 150 nm, the J–V curve is shown in Fig. 2. The J–V plot of the pure $Bepp_2$ film [23] is also shown in Fig. 2. There clearly show three distinct regions, unlike that of the pure $Bepp_2$ film: (1) Ohmic region, the slope of J–V plot in double logarithmic is about 1.13 at the lower voltage region (<0.5 V). (2) Space-charge limited conduction (SCLC) with discrete traps region, the slope of log J–log V plot is about 2.03 in the range of intermediate voltages.

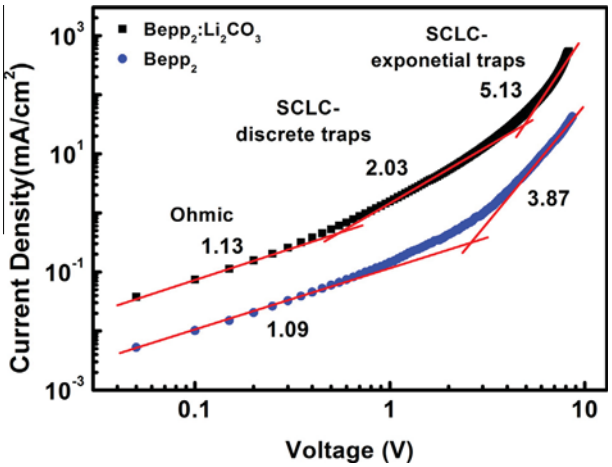

Fig. 2. J–V characteristics of pure $Bepp_2$ and $Bepp_2$:Li_2CO_3 films.

The current is relatively lower due to the presence of traps and quadratic field dependence is maintained in the case of discrete trap levels only. (3) SCLC with exponential trap distribution region, the slope of log J–log V plot is about 5.13 at higher voltages (>4.7 V). The current increases faster than quadratic due to the filling of trap states in the region. Fig. 3 shows d^2–V plot at J = 470 mA/cm^2. It can be seen that the quadratic thickness is proportional to the voltage, further indicating the exponential distribution of traps. Hence the current density (J) is given by [24],

$$J = q^{1-l}\mu N_v \left(\frac{2l+1}{l+1}\right)^{l+1} \left(\frac{l}{l+1}\frac{\varepsilon\varepsilon_0}{N_t}\right)^{l} \frac{V^{l+1}}{d^{2l+1}} \quad (1)$$

where q is the elementary charge, μ is the mobility, N_v is the density of states in the valence band, l is an energy parameter given by T_c/T (T_c is characteristic temperature of traps), N_t is the total density of traps, ε and ε_0 are dielectric constant and permittivity of free space, respectively, and d is the sample thickness. As an analytical method introduced by Kumar et al. [25] to determine N_t, Eq. (1) can be simplified as follows:

$$J = \frac{q\mu N_v V}{2d} \exp\left[-\frac{T_c}{T}\ln\left(\frac{qd^2N_t}{2\varepsilon\varepsilon_0 V}\right)\right] \quad (2)$$

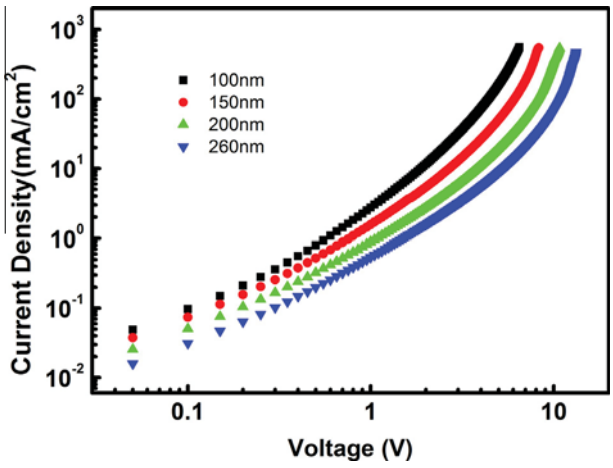

Fig. 1. Current density versus voltage (J–V) curves of $Bepp_2$:Li_2CO_3 films at different thicknesses.

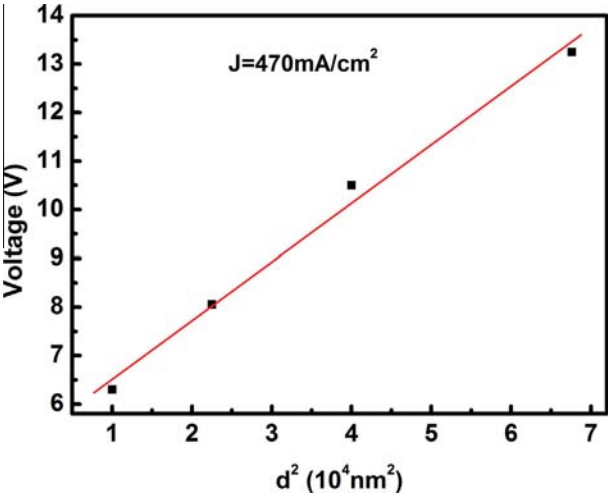

Fig. 3. Dependence of voltage on thickness in $Bepp_2$:Li_2CO_3 film in log–log scale at a current density of J = 470 mA/cm^2.

where $f(l) = \left(\frac{2l+1}{l+1}\right)^{l+1}\left(\frac{l}{l+1}\right)^{l}\frac{1}{2^l}$. For $l > 2$, $f(l) \approx 0.5$. On the base of the approximation, Eq. (2) can be written a typical Arrhenius form,

$$J = J_0 \exp\left(-\frac{E_a}{T}\right) \tag{3}$$

where, $J_0 = \frac{q\mu N_v V}{2d}$, $E_a = T_c \ln\left(\frac{qd^2 N_t}{2\varepsilon\varepsilon_0 V}\right)$. For $E_a = 0$, $J = J_0$, the current is independent of temperature. Finally, the I–V curves for various temperatures should congregate at a critical voltage,

$$V_c = \frac{qN_t d^2}{2\varepsilon\varepsilon_0} \tag{4}$$

Supposing $\varepsilon = 3$, it can be seen that only N_t and d determine V_c. By extrapolating log I–log V plots at different temperatures to higher voltages, we can obtain $V_c \approx 22$ V, as shown in Fig. 4. Then the value of N_t can be calculated as 3.24×10^{17} cm^{-3} by using Eq. (4).

3.2. Admittance properties

According to the studies of above J–V characteristics, the current in Li_2CO_3-doped $Bepp_2$ films is bulk-limited. Therefore, the AS measurements can be employed to study the electron transport properties in Li_2CO_3-doped $Bepp_2$ thin films. In this method, the current response i_{ac} to a small oscillating voltage $v_{ac} = v_0 \cos(\omega t)$ is monitored. The complex admittance $Y(\Omega)$ is related to i_{ac} and v_{ac} as follows: $Y(\Omega) = \frac{i_{ac}}{v_{ac}} = G(\omega) + i\omega C(\omega)$, where G, C and i are the conductance, capacitance and imaginary unit, respectively. $\omega = 2\pi f$ is the angular frequency. It is showed that $Y(\Omega)$ can be deduced analytically and is written by [26],

$$Y(\Omega) = \frac{\varepsilon\varepsilon_0 A}{\tau_{dc} d}\left\{\frac{\Omega^3}{2i[0.75\tilde{\mu}(\Omega)]^2[1-\exp(-i4(\Omega)/3\tilde{\mu}(\Omega))] + 1.5\tilde{\mu}(\Omega)\Omega - i\Omega^2}\right\} \tag{5}$$

In Eq. (5), ε and ε_0 respectively, are the dielectric constant of material and the permittivity of the free space. d and A are the thickness and the active area of the device, respectively. τ_{dc} is the carrier average transit time, which is directly related to the energy disorder of organic thin film, and the normalized frequency is defined by $\Omega = \omega\tau_{dc}$ .The frequency-dependent capacitance can be re-plotted as the negative differential susceptance $-\Delta B = -2\pi f(C - C_{geo})$, where the geometrical capacitance $C_{geo} = \varepsilon\varepsilon_0 A/d$. The plot typically yields a maximum of $-\Delta B$ at a characteristic frequency $f_r = 0.56/\tau_{dc}$. The carrier mobility can be then given by,

$$\mu_{dc} = \frac{f_r d^2}{0.56(V - V_{bi})} \tag{6}$$

where V is the applied bias voltage and V_{bi} is the built-in potential.According to the results of our experiment, the electron mobility of Li_2CO_3-doped $Bepp_2$ thin films can be extrapolated. Fig. 5 shows the C–f plots for the devices at room temperature. It is clear that the obtained C–f characteristic is different from that of pure $Bepp_2$ films (Fig. 6) [23]. For the pure $Bepp_2$ films, the capacitance is frequency independent and corresponds to the geometrical capacitance at zero bias voltage. In the low frequency ranges between 50 Hz and 4 kHz, however, for the case of Li_2CO_3-doped $Bepp_2$ thin films, the capacitance sharply decreased with frequency increase at zero applied bias voltage. The reasons are as follows. When the ac modulation signal is slowly enough to be followed by the trapping–detrapping process, the trap states begin to respond and induce additional capacitive contribution. At higher frequency (>8 kHz), the trap states cannot follow the ac modulation, the capacitance drops to a plateau, leaving the geometrical capacitance C_{geo} (~4 nF). Consequently, the relative dielectric constant of the Li_2CO_3-doped $Bepp_2$ thin films can be estimated as $\varepsilon = 4.2$. The value of N_t can be modified as 4.54×10^{17} cm^{-3} by Eq. (4). At the low frequency, with increasing the applied bias voltage the capacitance gradually decreases, and the decrease rate becomes slow. When a bias is applied to the electron-only device, the injected electrons will fill the trapped states, the numbers of trapped states decline. Furthermore, the electrons trapped in the discrete or shallow trap states recombine more efficiently with the free carriers, consequently, the capacitance of trap contribution is decreased more greatly in the low frequency range. Toward higher frequency (~1 MHz) the capacitance becomes little lower than the C_{geo}. As shown in the inset of Fig. 5, the behavior of capacitance at 3–8 V presents a minimum value, which is determined by the transit time [27]. In addition, negative capacitances are observed at lower frequencies when the applied voltage is more than 6 V. The negative capacitances shift to higher frequencies as increasing applied voltage. This is due to the space-charge relaxation transit time [28]. For a SCLC device, the injected carriers will relax to a new equilibrium space-charge distribution when a bias voltage is applied. The change of applied voltage leads to injection of additional space charge. The extra carriers result in an additional current. At low frequencies $\omega < \tau_{dc}^{-1}$, due to the finite τ_{dc}, the corresponding current lags behind the ac voltage. According to Eq. (5), the decreasing of $Y(\Omega)$ phase gives a negative contribution to the capacitance. At high

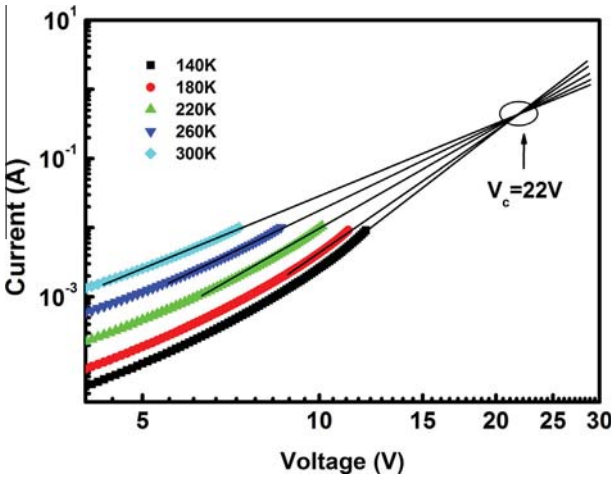

Fig. 4. Extrapolation of I–V plots at different temperatures in log–log scale for 150 nm thick $Bepp_2$:Li_2CO_3 device.

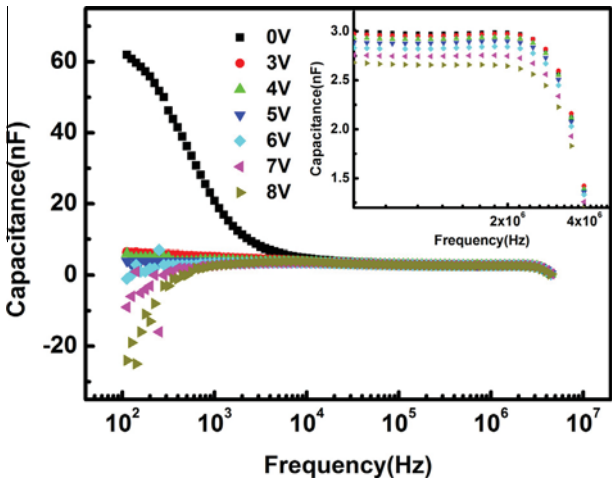

Fig. 5. Frequency dependence of capacitance of 150 nm thick $Bepp_2$:Li_2CO_3 film at the room temperature. The inset shows the dips in capacitance.

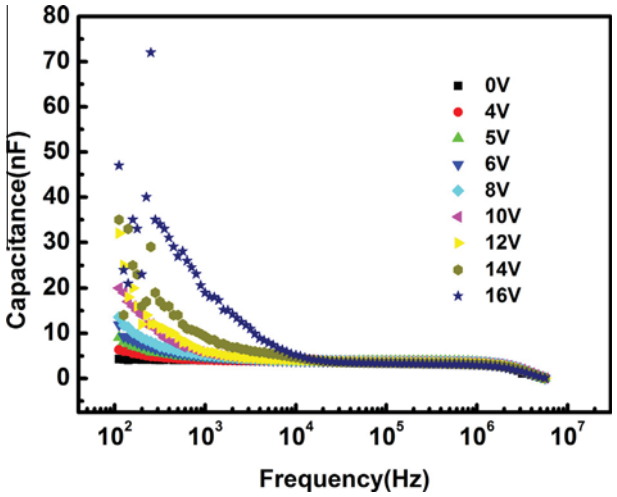

Fig. 6. Frequency dependence of capacitance of pure $Bepp_2$ film at the room temperature.

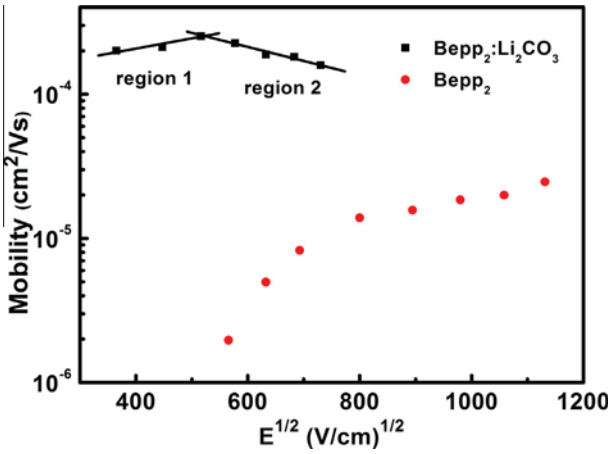

Fig. 8. Electron mobilities of pure $Bepp_2$ and $Bepp_2$:Li_2CO_3 films against the square root of the electric-field strength at room temperature.

frequencies, the injected carriers cannot respond to the frequency and the negative capacitance disappears. Hence, the capacitance equals the C_{geo}. Fig. 7 shows the $-\Delta B$–f plots for the electron-only device at room temperature. On the base of Eq. (6), the electron mobility can be calculated, which is shown in Fig. 8. The plot of mobility shows two linear parts: low electric field region (region 1) and high electric field region (region 2). At region 1, the mobility (2.01×10^{-4}–$2.52 \times 10^{-4}\,cm^2\,V^{-1}\,s^{-1}$) slightly increases with increasing the electric field. This increase should be the trapping effect of trap states. When the applied electric field increased, the trap depth can be decreased by Poole–Frenkel effect, leading to the increasing mobility. Whereas at region 2, the mobility (2.52×10^{-4}–$1.59 \times 10^{-4}\,cm^2\,V^{-1}\,s^{-1}$) slightly decreases as the electric field increases. The phenomenon of the slightly decreased mobility may be explained by the presence of certain energetic disorder [29,30]. For an along-field jump, when the fall of the electrostatic potential is comparable and even exceeds the energy barrier, the dwell time of a charge carrier on a site approaches the reciprocal rate for that jump because the jump reverse the field direction are gradually eliminated. Consequently, the transport velocity will saturate with the electric field. Correspondingly, the carrier average transit time τ_{dc} does not change with the increment of voltage. This demonstrates a linear decrease of the carrier mobility because it is controlled by energetically downward jump only that is not accelerated. In addition, the electron mobility of pure $Bepp_2$ thin film [23] is also shown in Fig. 8. Clearly, the electron mobility of Li_2CO_3-doped $Bepp_2$ thin film is almost two orders of magnitude higher than that of pure $Bepp_2$ thin film ($\sim 10^{-6}\,cm^2\,V^{-1}\,s^{-1}$). This implies that the electron mobility can be enhanced by doping Li_2CO_3, which is an effective way to balance the charge transport in an organic device.

3.3. Free electron density

Capacitance–voltage characteristics have been widely used to investigate the electrical and charge transport properties in organic diodes. Then the free charge carriers can be determined well by the capacitance–voltage characteristics [31–33]. In this case, the capacitance can generally be determined as [34]:

$$\frac{1}{C^2} = \frac{2(V_{bi} - V)}{A^2 q \varepsilon \varepsilon_0 N} \tag{7}$$

where V_{bi} is the built-in potential, A is the active area of the device, q is the elementary charge. ε and, ε_0 respectively, are the dielectric constant of material and the permittivity of the free space. In this

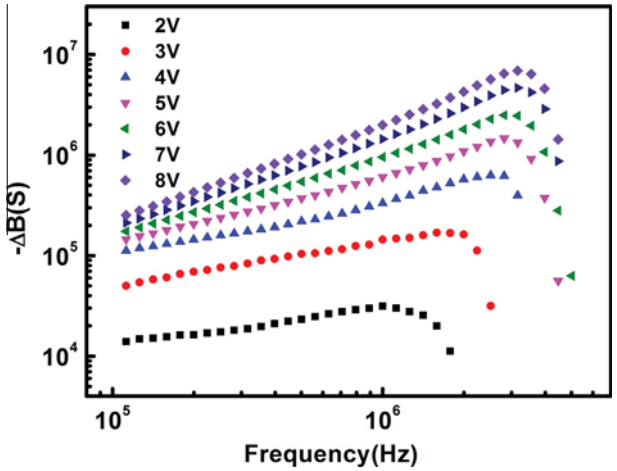

Fig. 7. Frequency dependence of the negative differential susceptance $-\Delta B$ of 150 nm thick $Bepp_2$:Li_2CO_3 film.

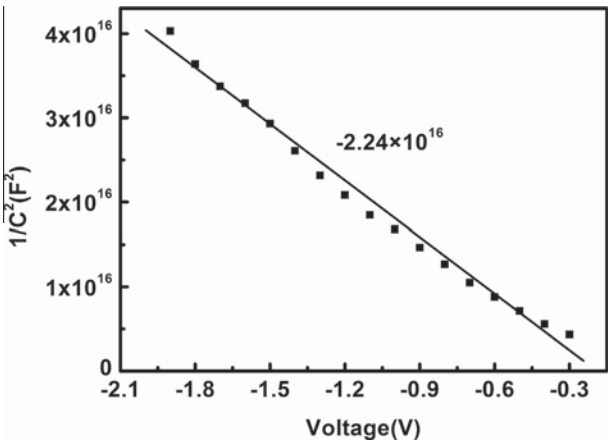

Fig. 9. $\frac{1}{C^2}$ vs. the bias voltage plot for 150 nm thick $Bepp_2$:Li_2CO_3 film at the room temperature.

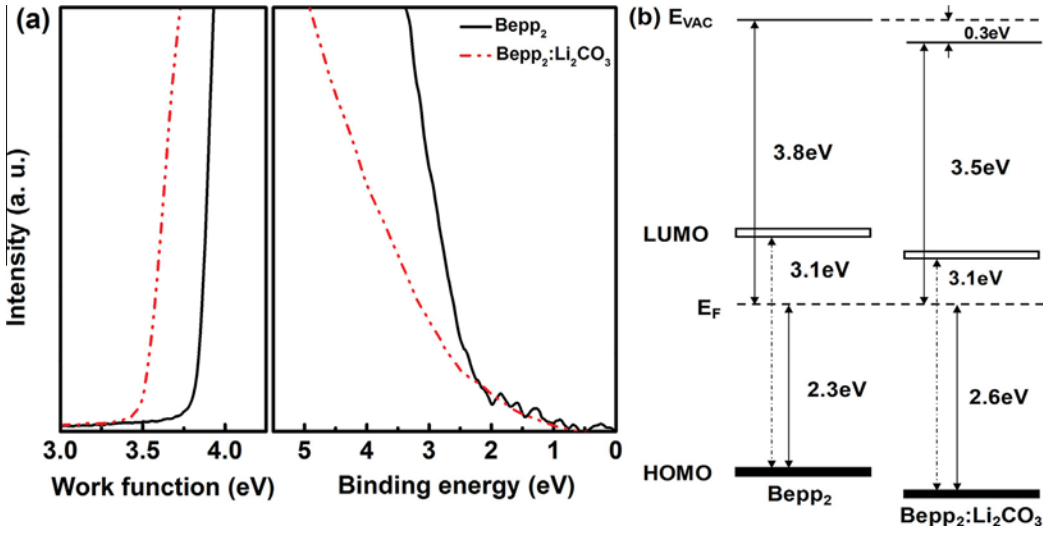

Fig. 10. (a) UPS spectra of pure $Bepp_2$ and $Bepp_2$:Li_2CO_3 film. Left: the low work function region showing the secondary electron cut-off; Right: valance band region near the Fermi energy. (b) Energy level diagrams of pure $Bepp_2$ and $Bepp_2$:Li_2CO_3 films.

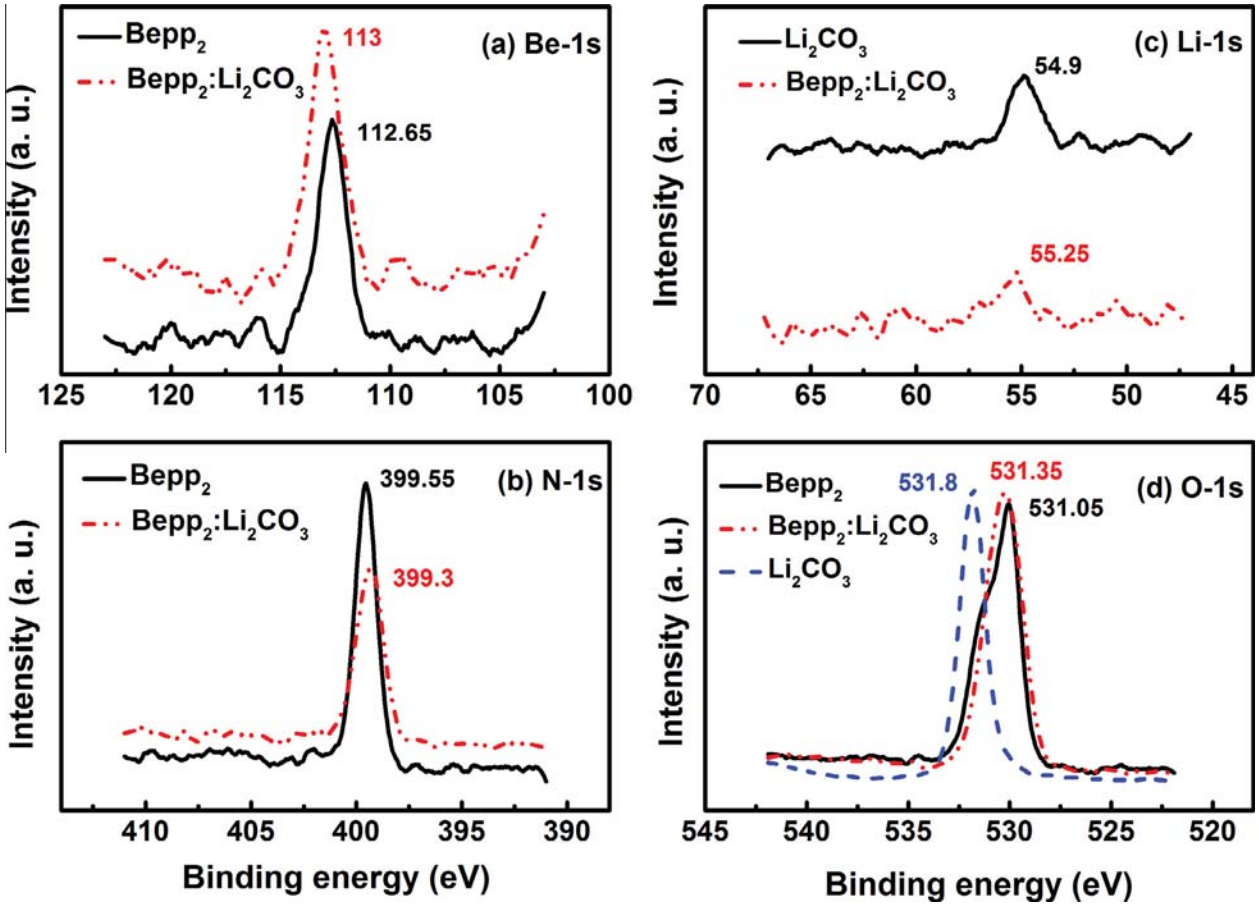

Fig. 11. XPS spectra of (a) Be 1s, (b) N 1s, (c) Li 1s and (d) O 1s of pure $Bepp_2$, pure Li_2CO_3 and $Bepp_2$:Li_2CO_3 films.

work, $\varepsilon = 4.2$. N is the active concentration of free charge carriers. $\frac{1}{C^2} \sim V$ plot for the Li_2CO_3-doped $Bepp_2$ thin film is shown in Fig. 9. It is found that the fitted line is in good agreement with $\frac{1}{C^2}$ versus the bias voltage plot, the slope is about -2.24×10^{16}. Then the value of N can be calculated as $5.85 \times 10^{16}\,cm^{-3}$ by using Eq. (7). It can be seen that N is much less than, N_t Eq. (1) is valid.

3.4. Electron mobility obtained by current–voltage characteristics

From Fig. 2, in the range of intermediate voltages, the electron transport in the Li_2CO_3-doped $Bepp_2$ thin film exhibits SCLC with discrete traps. The SCLC obeys the Mott-Gurney equation [35] modified by a factor θ,

$$J = \frac{9}{8}\theta\mu\varepsilon\varepsilon_0\frac{V^2}{d^3} \quad (8)$$

where the factor $\theta = \frac{N}{N+N_t}$ equals to the ratio of free carriers to the total number of carriers. Then the electron mobility can be obtained as 1.1×10^{-4} cm^2 V^{-1} s^{-1} by Eq. (8), which is approximately equal to that obtained by admittance spectroscopy.

3.5. UPS and XPS studies

To clearly demonstrate the electron injection and transport mechanism in Li_2CO_3-doped $Bepp_2$ thin films, UPS and XPS are employed to investigate the energy level and chemical compositions. Fig. 10(a) shows the UPS spectra of pure $Bepp_2$ and $Bepp_2$:Li_2CO_3 (3%) thin films. It can be seen that the work function is about 3.8 eV for pure $Bepp_2$. Nevertheless, for $Bepp_2$:Li_2CO_3 thin film, the work function is about 3.5 eV, indicating that the vacuum level of pure $Bepp_2$ thin film shifted down by 0.3 eV after doping Li_2CO_3. Furthermore, the edge of HOMO is about 2.3 eV below the Fermi level (E_F) for pure $Bepp_2$ thin film, and about 2.6 eV for $Bepp_2$:Li_2CO_3 thin film. This indicates that the E_F of pure $Bepp_2$ thin film shifted up by 0.3 eV due to doping Li_2CO_3. To give a good perception, the energy level diagrams of pure $Bepp_2$ and $Bepp_2$:Li_2CO_3 are shown in Fig. 10 (b). The bandgap of $Bepp_2$ is 3.1 eV which was obtained by standard electrochemical analysis method [36], we can estimate that the electron injection barrier of $Bepp_2$:Li_2CO_3 is about 0.5 eV less than that of pure $Bepp_2$ (0.8 eV). The level shift demonstrates that the electron injection barrier dropped as a result of n-type doping effect. It means that there are charge exchanges due to doping Li_2CO_3, which generate a considerable dipole field at the interface.

To further understand the charge exchanges mechanism in the Li_2CO_3-doped $Bepp_2$ film, the chemical compositions of pure $Bepp_2$, $Bepp_2$:Li_2CO_3 and pure Li_2CO_3 were studied by XPS, as shown in Fig. 8. As we can see from Fig. 11(a) and (b), when doping Li_2CO_3 into pure $Bepp_2$, the peaks of Be 1s and N 1s shift to higher and lower binding energy, respectively. From Fig. 11(c), it can be seen that the peak of Li 1s shifts to higher binding energy, comparing the XPS spectra of pure Li_2CO_3 and $Bepp_2$:Li_2CO_3 films. As shown in Fig. 11 (d), O 1s peak of Li_2CO_3-doped $Bepp_2$ film is between those of pure Li_2CO_3 and $Bepp_2$ films. Relatively, it shifts to lower binding energy and is closer to that of pure $Bepp_2$ films. The shift of binding energy indicates that there indeed occurs complicated chemical reaction between $Bepp_2$ and Li_2CO_3. The higher binding energies of the Be 1s and Li 1s mean the Be and Li atoms are charged positively, meanwhile, the lower binding energies of the N 1s and O 1s mean the some electrons being transferred to $Bepp_2$. According to the result of UPS and XPS, we can conclude that the $Bepp_2$ obtained more electrons than lost after Li_2CO_3 doping. This made the Fermi level move to the LUMO of $Bepp_2$, herein, the electron injection barrier is reduced and the electron mobility is increased.

4. Conclusions

We have studied the transport properties of an efficient n-type dopant of Li_2CO_3 into the organic semiconductor $Bepp_2$ by using AS measurements. The electron mobility is obtained from 1.59×10^{-4} to 2.52×10^{-4} cm^2 V^{-1} s^{-1} for the doping film, which is two orders of magnitude higher than that of pure $Bepp_2$ film ($\sim 10^{-6}$ cm^2 V^{-1} s^{-1}). The current–voltage characteristics show that the electron conduction is SCLC with discrete trap distributions in the intermediate voltage range and SCLC with exponential trap distribution at higher voltages, implying that the electron conduction is mainly charged by traps. Hence, the electron mobility is nearly independent on the electric field. The density of trap states is estimated as about 4.54×10^{17} cm^{-3} by the temperature dependent current density characteristics. Moreover, the electron transport properties and mechanism have been investigated by UPS and XPS. The results demonstrate that charge exchange between $Bepp_2$ and Li_2CO_3 is a complicated process. Ultimately, there occurs electron transfer from Li_2CO_3 to $Bepp_2$, which reduces the electron injection barrier and enhances the electron mobility. This clearly explains the reason why Li_2CO_3 doping in organic semiconductors can greatly improve the performance of organic optoelectronic devices.

Acknowledgements

The authors gratefully acknowledge the National Natural Science Foundation of China (51333007, 91433201, 61204059), Ministry of Science and Technology of China (973 program No. 2013CB834805), the Foundation of Jilin Research Council (2012ZDGG001, 20130206003GX), Chinese Academy of Sciences (KGZD-EW-303-3) for the support of this research.

References

[1] C.W. Tang, S.A. VanSlyke, Appl. Phys. Lett. 51 (1987) 913.
[2] S.R. Forrest, Nature 428 (2004) 911.
[3] H.B. Wu, G.J. Zhou, J.H. Zou, Cheuk-Lam Ho, Wai-Yeung Wong, W. Yang, J.B. Peng, Y. Cao, Adv. Mater. 21 (2009) 1.
[4] N. Sun, Q. Wang, Y.B. Zhao, Y.H. Chen, D.Z. Yang, F.C. Zhao, J.S. Chen, D.G. Ma, Adv. Mater. 26 (2014) 1617.
[5] C.W. Tang, Appl. Phys. Lett. 48 (1986) 183.
[6] A.J. Medford, M.R. Lilliedal, M. Jørgensen, D. Aarø, H. Pakalski, J. Fyenbo, F.C. Krebs, Opt. Express 18 (2010) A272.
[7] Z.J. Wang, Y. Wu, Y.C. Zhou, J. Zhou, S.J. Zhang, X.M. Ding, X.Y. Hou, Z.Q. Zhu, Appl. Phys. Lett. 88 (2007) 222112.
[8] S.F. Chen, Y.K. Fang, S.C. Hou, C.Y. Lin, W.R. Chang, T.H. Chou, Org. Electron. 6 (2005) 92.
[9] J. Huang, M. Pfeiffer, A. Werner, J. Blochwitz, K. Leo, S. Liu, Appl. Phys. Lett. 80 (2002) 139.
[10] S. Noh, C.K. Suman, Y. Hong, C.H. Lee, J. Appl. Phys. 105 (2009) 033709.
[11] J. Blochwitz, M. Pfeiffer, T. Fritz, K. Leo, Appl. Phys. Lett. 73 (1998) 729.
[12] K.R. Choudhury, J.H. Yoon, F. So, Adv. Mater. 20 (2008) 1456.
[13] Po-Ching Kao, Jie-Han Lin, Jing-Yuan Wang, Cheng-Hsien Yang, Sy-Hann Chen, J. Appl. Phys. 109 (2011) 094505.
[14] J. Zhao, Y. Cai, J.-P. Yang, H.-X. Wei, Y.-H. Deng, Y.-Q. Li, S.-T. Lee, J.-X. Tang, Appl. Phys. Lett. 101 (2012) 193303.
[15] M.-H. Ho, T.-M. Chen, P.-C. Yeh, S.-W. Hwang, C.H. Chen, Appl. Phys. Lett. 91 (2007) 233507.
[16] S.-Y. Chen, T.-Y. Chu, J.-F. Chen, C.-Y. Su, C.H. Chen, Appl. Phys. Lett. 89 (2006) 053518.
[17] F. Huang, P.I. Shih, C.F. Shu, Y. Chi, A.K.Y. Jen, Adv. Mater. 21 (2009) 361.
[18] S. Ishihara, H. Hase, T. Okachi, H. Naito, Org. Electron. 12 (2011) 1364.
[19] O.S. Elsherif, K.D. Vernon-Parry, I.M. Dharmadasa, J.H. Evans-Freeman, R.J. Airey, M.J. Kapper, C.J. Humphreys, Org. Electron. 520 (2012) 3064.
[20] I.N. Hulea, R.F.J. van der Scheer, H.B. Brom, Appl. Phys. Lett. 83 (2003) 1246.
[21] D. Poplavskyy, F. So, J. Appl. Phys. 99 (2006) 033707.
[22] L. Burtone, J. Fischer, K. Leo, M. Riede, Phys. Rev. B. 87 (2013) 045432.
[23] Y.P. Wang, J.S. Chen, J.Y. Huang, D.G. Ma, L.S. Dong, H. Chen, J. Appl. Phys. 115 (2014) 223707.
[24] M.A. Lampert, P. Mark, Current Injection in Solids, Academic Press, New York, 1970.
[25] V. Kumar, S.C. Jain, A.K. Kapoor, J. Poortmans, R. Mertens, J. Appl. Phys. 94 (2003) 1283.
[26] S.W. Tsang, S.K. So, J.B. Xu, J. Appl. Phys. 99 (2006) 013706.
[27] J. Shao, G.T. Wright, Solid-State Electron. 3 (1961) 291.
[28] (a) H.C.F. Martens, H.B. Brom, P.W.M. Blom, Phys. Rev. B 60 (1999) R8489–R8492;
(b) H.H.P. Gommans, M. Kemerink, R.A.J. Janssen, Phys. Rev. B 72 (2005) 235204.
[29] A.J. Mozer, N.S. Sariciftci, A. Pivrikas, R. Österbacka, G. Juška, L. Brassat, H. Bässler, Phys. Rev. B 71 (2005) 035214.
[30] K. Seki, M. Tachiya, Phys. Rev. B 65 (2001) 014305.
[31] M.E. Aydin, F. Yakuphanoglu, J.-H. Eom, D.-H. Hwang, Physica B 387 (2007) 239.
[32] A. Rihani, N. Boutabba, L. Hassine, S. Romdhane, H. Bouchriha, Synth. Met. 145 (2004) 129.
[33] W.-J. Shin, J.-Y. Lee, J.C. Kim, T.-H. Yoon, T.-S. Kim, O.-K. Song, Org. Electron. 9 (2008) 333.
[34] S.M. Sze, Physics of Semiconductor Devices, second ed., Wiley-Interscience, New York, 1981.
[35] N.F. Mott, R.W. Gurney, Electronic Processes in Ionic Crystals, Clarendon Press, Oxford, 1940.
[36] Y.Q. Li, Y. Liu, J.H. Guo, F. Wu, W.J. Tian, B.F. Li, Y. Wang, Synth. Met. 118 (2001) 175.